Fluid dynamics and heat transfer with phase change of multiple spherical droplets in a laminar axisymmetric gas stream

C. Kleinstreuer, J. K. Comer and H. Chiang*
Department of Mechanical and Aerospace Engineering, North Carolina State University, Raleigh, NC, USA

The transient gas–liquid velocity and temperature fields of interacting vaporizing n-hexane fuel droplets and water droplets have each been analyzed for two sets of representative initial conditions. Laminar axisymmetric flow and three spherical droplets are the key assumptions for the present finite-element solution. During the start-up phase, *fuel* droplets exhibit dramatic changes in fluid properties and interfacial quantities, notably the individual vaporization rates and tangential velocities, which largely determine the multiple-droplet behavior. The gas-phase velocity/temperature fields and liquid-phase streamlines/isotherms shown reflect in detail the transient droplet interaction characteristics such as thick boundary layers, weak recirculation zones between pairing droplets, and vortex-dominated droplet temperature fields. In contrast, the dynamics of interacting *water* droplets is much less visible and takes far longer to develop than for (n-hexane) fuel droplets.

Keywords: interacting vaporizing polydisperse droplets; laminar axisymmetric flow; complete transport equations; finite-element solution of two-phase velocity and temperature fields

Introduction

Of interest are the transient two-phase flow dynamics and heat transfer of interacting vaporizing fuel and water droplets. A detailed solution to this gas–liquid flow problem is the stepping stone for a better understanding of the interfacial transfer processes. These, in turn, largely determine droplet behavior in the dense spray region and hence influence design and/or operational aspects of droplet atomizers. Such considerations are important in numerous spray applications, for example, fuel droplet or liquid waste combustion, flue gas desulfurization, aerosol microphysics, spray cooling, spray coating, and agricultural sprays. *Dense* high-temperature sprays are characterized by close droplet proximities resulting in dynamic droplet and droplet streamer interactions, Reynolds numbers of $\mathcal{O}(100)$, initial liquid-phase heating, internal droplet circulation, rapid droplet vaporization, and variable fluid properties. The dense regime is followed by a *dilute* spray region where droplet–droplet interactions are negligible, but the other coupled effects still have an influence. Additional complexities of droplet sprays are discussed elsewhere (cf. Clift et al. 1978; Sirignano 1983; Kuo 1986; Law 1990).

Presently, the state-of-the-art in *numerical* dense-spray analysis includes a couple of stochastic modeling approaches (cf. Bracco 1985; Faeth 1987), several deterministic approaches using the spherical cell model (cf. Tal et al. 1984) for droplet clusters or numerical solutions of the complete transport equations for steady or transient laminar flow past single evaporating droplets (cf. Renksizbulut and Haywood 1988; Chiang et al. 1989), or two droplets in tandem (cf., Raju and Sirignano 1990). The two-droplet study by Raju and Sirignano (1990) assumes constant transport properties and focuses on criteria for potential droplet collision (or permanent separation) for different initial droplet spacings and size ratios. Approximate, boundary-layer type analyses of multiple droplets for free-stream Reynolds numbers $Re_d > 100$ have been discussed by Abramizon and Sirignano (1988) and Kleinstreuer and Wang (1990). *Experimental* dense-spray analysis is almost nonexistent except for a few visualizations of two or more closely spaced solid spheres (cf. Rowe and Henwood 1961; Tsuji et al. 1983). Renksizbulut and Yuen (1983) provided empirical Nusselt number correlations for a single sphere with blowing, and Mulholland et al. (1988) recorded two-dimensional (2-D) trajectories of nonevaporating water drops.

In this paper, which is based on our previous contributions (cf. Ramachandran et al. 1987; Kleinstreuer et al. 1990; Kleinstreuer et al. 1989; Ramachandran et al. 1991; Chiang and Kleinstreuer 1991; Chiang and Kleinstreuer 1992), the highly coupled, nonlinear dense-spray characteristics listed above are simulated with a *representative* system of three decelerating, spherically shrinking droplets in a laminar axisymmetric heated gas stream. For an initial gas-phase Reynolds number of $Re_o = 100$, the time histories of the two-phase flow fields and associated temperature contours are analyzed for fuel (n-hexane) droplets and water droplets.

Analysis

Considering three spherical droplets decelerating and evaporating on a one-dimensional (1-D) trajectory in a high-temperature, dry-air environment, the gas-phase momentum,

* Presently with ITR Institute, Thermofluid Technology Division, Taiwan, Republic of China
Address reprint requests to Professor Kleinstreuer at the Department of Mechanical and Aerospace Engineering, North Carolina State University, Raleigh, NC 27695, USA.

Received 5 October 1991, accepted 15 December 1992

heat, and mass transfer equations are coupled with the liquid-phase momentum and heat transfer equations via the interfacial compatibility conditions. Gas-phase turbulence, nonsphericity, thermal radiation, buoyancy and thermodiffusion effects are neglected (cf., Clift et al. 1978; Chiang 1991). Thus, the dimensionless equations for laminar thermal flow with variable fluid properties can be written as follows (cf. Figure 1).

Gas phase

$$\frac{\partial \rho_g}{\partial \tau} + \nabla \cdot (\rho_g \vec{v}_g) = 0 \tag{1}$$

$$\left(\frac{\partial}{\partial \tau} + \vec{v}_g \cdot \nabla\right)(\rho_g \vec{v}_g) = -\nabla p_g + \mathrm{Re}_g^{-1} \nabla \cdot (\chi_g \nabla \vec{v}_g) \tag{2}$$

$$\left(\frac{\partial}{\partial \tau} + \vec{v}_g \cdot \nabla\right)(\rho_g \eta_g T_g) = \mathrm{Pe}_{h,g}^{-1} \nabla \cdot (\lambda_g \nabla T_g) + \rho_g \left(\frac{c_{p,v} - c_{p,a}}{c_{p\infty}}\right) \mathrm{Pe}_{m,g}^{-1} \omega_g (\nabla T_g \cdot \nabla Y_g) \tag{3}$$

$$\left(\frac{\partial}{\partial \tau} + \vec{v}_g \cdot \nabla\right)(\rho_g Y_g) = \mathrm{Pe}_{m,g}^{-1} \nabla \cdot (\rho_g \omega_g \nabla Y_g) \tag{4}$$

Liquid phase

$$\frac{\partial \rho_l}{\partial \tau} + \nabla \cdot (\rho_l \vec{v}_l) = 0 \tag{5}$$

$$\left(\frac{\partial}{\partial \tau} + \vec{v}_l \cdot \nabla\right)(\rho_l \vec{v}_l) = -\nabla p_l + \mathrm{Re}_l^{-1} \nabla \cdot (\chi_l \nabla \vec{v}_l) \tag{6}$$

$$\left(\frac{\partial}{\partial \tau} + \vec{v}_l \cdot \nabla\right)(\rho_l \eta_l T_l) = \mathrm{Pe}_{h,l}^{-1} \nabla \cdot (\lambda_l \nabla T_l) \tag{7}$$

where

$$\vec{v} = \vec{v}^*/u_o^*, \quad p = p^*/(\rho_\infty^* u_o^{*2}), \quad T = T^*/T_\infty^*, \quad \nabla = \nabla^* d_o^*,$$

$$\tau = t^* u_o^*/d_o^*, \quad \rho = \rho^*/\rho_r^*, \quad \eta = c_p^*/c_{p,r}^*, \quad \chi = \mu^*/\mu_r^*,$$

$$\lambda = k^*/k_r^*, \quad \omega = \mathscr{D}^*/\mathscr{D}_r^*, \quad \mathrm{Re}_o = u_o^* d_o^*/\nu_r^* \quad \mathrm{Pe}_h = u_o^* d_o^*/\alpha_r^*,$$

$$\text{and} \quad \mathrm{Pe}_m = u_o^* d_o^*/\mathscr{D}_r^* \tag{8a–m}$$

The dimensional quantities are starred where u_o^* is the initial free-stream or initial droplet velocity; d_o^* is the initial droplet diameter; and subscript ∞ indicates (updated) conditions at infinity, while subscript r means reference value. The reference fluid properties are evaluated at the free-stream conditions for the gas-phase parameters, and for the liquid phase, the initial droplet temperature is chosen as reference. The second term

Notation

a	Radius of droplet
c_p	Heat capacity
C_D	Drag coefficient
d	Droplet diameter
d_{ij}	Dimensionless interdroplet distances, $d_{ij} = d_{ij}^*/d_o^*$
$\mathscr{D}$	Diffusion coefficient
k	Thermal conductivity
Le	Lewis number, Sc/Pr
M	Molecular weight
p	Pressure
Pr	Prandtl number, ν/α
Pe	Peclet number, Re Pr
q_h''	Dimensionless interfacial heat flux
q_m''	Dimensionless interfacial mass flux
r	Radial spherical coordinate
R	Radial cylindrical coordinate
Re_o	Initial Reynolds number, $u_o^* d_o^*/\nu$
Re	Instantaneous Reynolds number, $u^* d^*/\nu$
Sc	Schmidt number, $\nu/\mathscr{D}$
t	Time
T	Temperature
$\vec{v}$	Velocity vector
u_n, v_n	Normal or local blowing velocity
u_t, v_t	Tangential components
u, v	Velocity components
u_∞	Instantaneous free stream velocity
u_o	Initial free stream velocity
$\forall$	Volume, variable
X	Mole fraction
Y	Mass fraction
Z	Axial cylindrical coordinate

Greek symbols

α	Thermal diffusivity; drag coefficient ratio
η	Heat capacity ratio
θ	Spherical coordinate
λ	Thermal conductivity ratio
μ	Dynamic viscosity
ν	Kinematic viscosity
ξ	Density ratio
ρ	Density
τ	Dimensionless time, tu_o^*/d_o^*
τ_s	Surface shear stress
χ	Dynamic viscosity ratio
ω	Mass diffusivity ratio

Subscripts

a (air; 1)	Air
bp	Boiling point
f	Fuel
g	Gas phase
h	Heat transfer
i	Index for particle spacing ($i = 1, 2$)
j	Index for particle spacing ($j = i + 1$)
k	Index for particle identification ($k = 1, 2, 3$)
l	Liquid phase
m	Mass transfer
n	Normal direction
o	Initial, reference
p	Pressure
r, ref	Reference
s	Surface; single
t	Tangential direction
v	Vapor
w	Water
∞	(Instantaneous) Free-stream quantity

Superscripts

(k)	Index for particle identification ($k = 1, 2, 3$)
*	Dimensional quantities

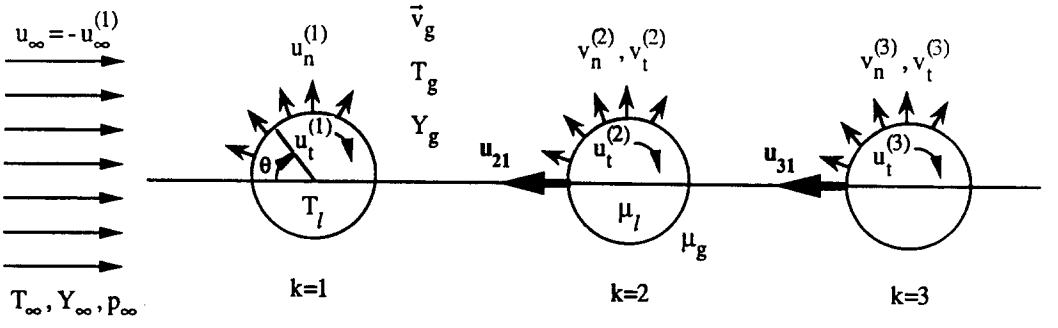

Figure 1 Schematics for vaporizing interacting droplets on a 1-D trajectory

on the right-hand side of Equation 3 is the interdiffusion term, which represents the net enthalpy effect between fuel or water vapor and dry air.

The fixed origin of the axisymmetric coordinates (R, Z) is located at the center of the first droplet. The gas flow field, a cylindrical domain, is evaluated separately from the liquid-phase, i.e., the spherical domain. Thus, the flow field considered here is 2-D axisymmetric. Coupling of the two fluid flow fields at each time step is described below. At $\tau = 0$, when the first droplet is being injected into the ambient, the gas phase is characterized by its initial velocity, temperature, and vapor concentration fields, while the liquid phase is stagnant and at its initial temperature. At the domain inlet,

$$u_g = 1, \quad v_g = 0, \quad T_g = 1, \text{ and } Y_g = 0 \tag{9a–d}$$

Because of symmetry, all gradients at the centerline ($R = 0$) are equal to zero. The extent of the computational domain, being a function of the free-stream Reynolds number (cf. Chiang and Kleinstreuer 1992), is large enough so that all appropriate outer boundary and outlet gradients are equal to zero.

Compatibility conditions

Both phases are coupled via the interfacial conditions representing conservation of mass, momentum, and energy. Specifically, continuous velocities, shear stress, and temperature are required at the gas–liquid boundaries.

$$u_{t,g} = u_{t,l}, \quad \tau_{s,g} = \left(\frac{\rho_{o,l}}{\rho_{\infty,g}}\right)\tau_{s,l}, \text{ and } \quad T_{s,g} = T_{s,l} \tag{10a–c}$$

where

$$\tau_s = \frac{\chi}{\mathrm{Re}} \frac{\partial u}{\partial r}\bigg|_{r=a(\tau)} \tag{10d}$$

The normal interfacial velocity, i.e., the vapor blowing velocity, is proportional to the dimensionless diffusion mass flux

$$u_{n,g} = \frac{1}{1 - Y_s} q''_{m,g} = -\frac{1}{1 - Y_s}\left(\frac{\omega_g}{\mathrm{Pe}_{m,g}} \frac{\partial Y}{\partial r}\right)\bigg|_{r=a(\tau)} \tag{11}$$

where Y_s is the vapor concentration at the droplet surface assuming thermodynamic equilibrium:

$$Y_s = \frac{M_v X_s}{M_v X_s + M_a(1 - X_s)} \tag{12a}$$

where the interfacial mole fraction

$$X_s = p_{v,s}(T_s)/p_a \tag{12b}$$

The heat transferred from the gas stream divides up into liquid droplet heating and latent heat of vaporization:

$$q''_{h,g} = \gamma q''_{h,l} + \frac{\xi_g}{1 - Y_s} \frac{c_{p\infty,g} T_\infty}{L(T_s)} q''_{m,g} \tag{13a}$$

where

$$\gamma = \frac{\rho_{o,l} c_{po,l}}{\rho_{\infty,g} c_{p\infty,g}}, \quad q''_h = -\lambda \mathrm{Pe}_h^{-1} \frac{\partial T}{\partial r}\bigg|_{r=a(\tau)} \tag{13b,c}$$

and

$$q''_m = -\omega\, \mathrm{Pe}_m^{-1} \frac{\partial Y}{\partial r}\bigg|_{r=a(\tau)} \tag{13d}$$

Auxiliary conditions

Assuming spherical droplets at all times, the decrease in each droplet radius with time, or shrinkage, can be expressed as

$$\frac{da^{(k)}}{d\tau} = \frac{\rho_g}{2\rho_l} \int_0^\pi u_{n,g}^{(k)} \sin\theta \, d\theta \tag{14}$$

where the superscript k identifies each droplet, i.e., $k = 1$, 2, 3.

The deceleration of each droplet due to the gas-phase drag force can be described by Newton's second law of motion, as

$$m^{(k)} \frac{du_\infty^{*(k)}}{dt^*} = -\frac{\pi (a^{*(k)})^2}{2} \rho_{\infty,g} (u_\infty^{*(k)})^2 \hat{C}_D^{(k)} \tag{15a}$$

Nondimensionalization yields

$$\frac{du_\infty^{(k)}}{d\tau} = -\frac{3}{8}\left(\frac{\rho_{\infty,g}}{\bar{\rho}_l^{(k)}}\right)\left(\frac{a_o}{a^{(k)}(\tau)}\right)(u_\infty^{(k)})^2 \hat{C}_D^{(k)} \tag{15b}$$

where $\hat{C}_D^{(k)}$ is the drag coefficient of droplet k based on the *instantaneous* droplet velocity, $u_\infty^{(k)}$. For convenience, the initial droplet injection speed, u_o^*, should be employed, where $\hat{C}_D^{(k)}/u_o^{*2} = C_D^{(k)}/(u_\infty^{*(k)})^2$. Thus,

$$\frac{du_\infty^{(k)}}{d\tau} = -\frac{3}{8}\left(\frac{\rho_{\infty,g}}{\bar{\rho}_l^{(k)}}\right)\left(\frac{a_o}{a^{(k)}(\tau)}\right) C_D^{(k)} \tag{15c}$$

where $\bar{\rho}^{(k)} \approx \rho_{o,l}$ for simplicity and $C_D^{(k)}$ is discussed below.

In the Eulerian frame chosen, the free-stream gas flow approaches the leading droplet with a velocity of $u_\infty = -u_\infty^{(1)}$. Since each droplet is subjected to a different drag force, the instantaneous velocity of each droplet can be written as

$$u_\infty^{(k)} = \tilde{u}_\infty^{(k)} + \Delta u^{(k)}; \quad k = 1, 2, 3 \tag{15d}$$

which is obtained from Equation 15c after integration. Velocities u_∞ and $\tilde{u}_\infty$ are evaluated at the new and previous

Table 1 Liquid- and gas-phase fluid properties at reference conditions

$p_\infty = 10$ atm $T_\infty = 1200$K $T_o = 350$K	ρ $\left(\frac{kg}{m^3}\right)$	c_p $\left(\frac{kJ}{kgK}\right)$	k $\left(\frac{kW}{m \cdot K}\right)$	μ $\left(\frac{N \cdot sec}{m^2}\right)$	M_v (—)	T_{bp} (K)	$\mathcal{D}$ $\left(\frac{m^2}{sec}\right)$
n-hexane (liq.)	0.6508E + 2	2.451	1.106E − 4	1.918E − 4	86	438	6.903E − 6
gas (at infinity)	2.911	1.143	7.046E − 5	4.775E − 5	—	—	—
$p_\infty = 1$ atm $T_\infty = 800$K $T_o = 330$K	ρ $\left(\frac{kg}{m^3}\right)$	c_p $\left(\frac{kJ}{kgK}\right)$	k $\left(\frac{kW}{m \cdot K}\right)$	μ $\left(\frac{N \cdot sec}{m^2}\right)$	M_v (—)	T_{bp} (K)	$\mathcal{D}$ $\left(\frac{m^2}{sec}\right)$
water (liq.)	9.950E + 2	4.204	6.594E − 4	4.777E − 4	18	372	0.216
gas (at infinity)	0.4354	1.117	5.711E − 5	3.695E − 4	—	—	—

time steps, respectively, and Δu is the velocity variation during the time increment.

The velocity of the second droplet with respect to the leading droplet is

$$\begin{aligned} u_{21} &= u_\infty^{(2)} - u_\infty^{(1)} \\ &= (\tilde{u}_\infty^{(2)} + \Delta u^{(2)}) - (\tilde{u}_\infty^{(1)} + \Delta u^{(1)}) \\ &= (\tilde{u}_\infty^{(2)} - \tilde{u}_\infty^{(1)}) + (\Delta u^{(2)} - \Delta u^{(1)}) \\ &= \tilde{u}_{21} + \Delta u_{21} \end{aligned} \tag{15e}$$

Similarly for the third droplet,

$$\begin{aligned} u_{31} &= u_\infty^{(3)} - u_\infty^{(1)} \\ &= \tilde{u}_{31} + \Delta u_{31} \end{aligned} \tag{15f}$$

The motions of the second and third droplets relative to the leading droplet must show their effect on the entire gas flow field. Hence, the modifications of the boundary conditions are

$$v_n^{(k)} = u_n^{(k)} + u_{k1} \cos\theta \tag{15g}$$

$$v_t^{(k)} = u_t^{(k)} - u_{k1} \sin\theta \qquad k = 2, 3 \tag{15h}$$

Here, u_n and u_t are the liquid-phase surface blowing velocity and tangential velocity, respectively, while v_n and v_t are the modified boundary conditions required for the second and third droplet. The relationship of these velocities are shown in Figure 1. Fluid property correlations are given in Chiang and Kleinstreuer (1992). Reference data for the different fluids are given in Table 1.

Numerical solution

The governing equations (Equations 1–7), subject to the conditions in Equations 9–17, are solved using a modified and extended finite-element software package (cf. Engelman 1990; Chiang 1991). For this convective-dominated flow problem, nine-node isoparametric quadrilateral elements are used (cf. Cuvelier et al. 1986). Bilinear shape functions are selected for the pressure approximations, while biquadratic shape functions are employed for the other field variables. Very small elements are placed and updated at the receding interface, where $\Delta\theta = 3.2°$, and large elements are located near the domain boundaries. A smooth transition from fine to coarse mesh regions has been achieved. For the multiple droplet systems, mesh renewal is not only necessary in the radial direction because of droplet shrinking, but also in the axial direction following the relative motion of the second and third droplet with respect to the fixed frame at the center of the lead droplet. In order to maintain uniform mesh distributions for every time step, interpolations of the field variables (i.e., velocity, temperature, and concentration) are made at the end of each time step so that computations can be continued with the new mesh. A variable, rather small time step is used (i.e., $0.5 \leq \Delta\tau \leq 10$) for the multiple droplet system in order to minimize "false diffusion" caused by interpolations. The overall mesh size has been obtained in accordance with the boundary conditions by trial and error. Independence of the simulation results from the mesh density has been successfully tested based on repeat calculations with finer meshes, i.e., a further mesh refinement would not have improved the present results. The resulting mesh data include 216 elements or 913 nodes for each droplet and 1440 elements or 6015 nodes for the gas phase.

The solution is started with the calculation of the gas-side interfacial shear stress, heat flux, and mass flux in order to evaluate the liquid-phase velocity and temperature distributions. Matching of the interfacial boundary conditions has been obtained within six iterations, where $\varepsilon = |\forall^{new} - \forall^{old}| < 10^{-5}$, using an underrelaxation coefficient of 0.6 to 0.7. All fluid properties are constantly updated with the new local temperatures and vapor concentrations. As mentioned in the preceding section, the two-phase regions are solved sequentially because of their different convergence requirements and for reasons of computational efficiency. For example, since the liquid phase is subjected to Neumann-type boundary conditions, a more stable but slower iteration scheme, i.e., the successive substitution method, has been applied. Furthermore, instead of solving a very large system of combined gas-phase *and* liquid-phase equations, the *segregated* solution procedure requires less computer time without sacrificing accuracy. Each droplet is updated individually because of its unique scales of the salient transfer mechanisms. However, calculations for both regions progress with common time steps, typically dictated by the more rapidly changing gas phase. Necessary local mesh regeneration due to droplet shrinking and adjustment of the inlet free-stream (or droplet) velocity due to droplet deceleration are performed at the end of each time step. An inertia term for Equation 15b, as suggested by Chiang et al. (1989), was found to be insignificant in this study. The computational procedure was terminated after about 50 percent of the droplet mass had been evaporated or imminent

collision had been observed. A complete case run takes about 8 hours of CPU time for a single vaporizing droplet, and about 12 hours for the three-droplet system on a CRAY Y-MP. Future use of a conjugate-gradient-based iterative solver will reduce run times of this large problem significantly. Alternatively, utilization of parallel processing capabilities of high-end workstations may eliminate the need of a supercomputer altogether.

Results and discussion

Computer simulations of the dynamics of interacting vaporizing droplets were carried out for two liquids, i.e., n-hexane and water (cf. Table 1). In selecting appropriate sets of initial conditions for the fuel and water droplets, all initially at $Re_o = 100$, the contrasting temporal changes of differential and integral quantities were then examined. The accuracy of the present finite-element code has been successfully documented for single and two spheres/drops in our previous publications (cf. Kleinstreuer et al. 1989; Ramachandran et al. 1991; Chiang and Kleinstreuer 1991; Chiang and Kleinstreuer 1992).

When (fuel) vapors of relatively high molecular weight are injected into a heated gaseous ambient, the local, instantaneous density and specific heat capacity strongly influence the gas-phase temperature near the interface. Furthermore, the mass diffusion coefficients for fuel vapor through air are temperature dependent, i.e., $\mathscr{D} \sim T^{1.6}$. As a result, the Lewis number, based on interfacial conditions and relating thermal diffusion to mass diffusion, differs significantly from unity during the early stages ($\tau_f < 50$) of fuel droplet heating (cf. Figure 2a). In contrast, the Lewis number for water stays around $Le \approx 0.805$ during the (transient) process (cf. Figure 2b). Hence, the assumption of constant fluid properties for vaporizing *water* droplets is quite adequate.

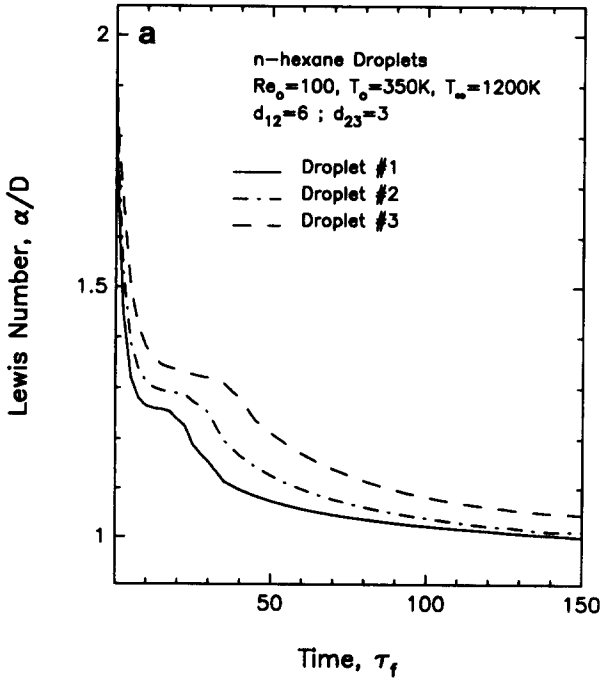

Figure 2(a) Transient Lewis numbers for n-hexane fuel droplets ($p_\infty = 10$ atm)

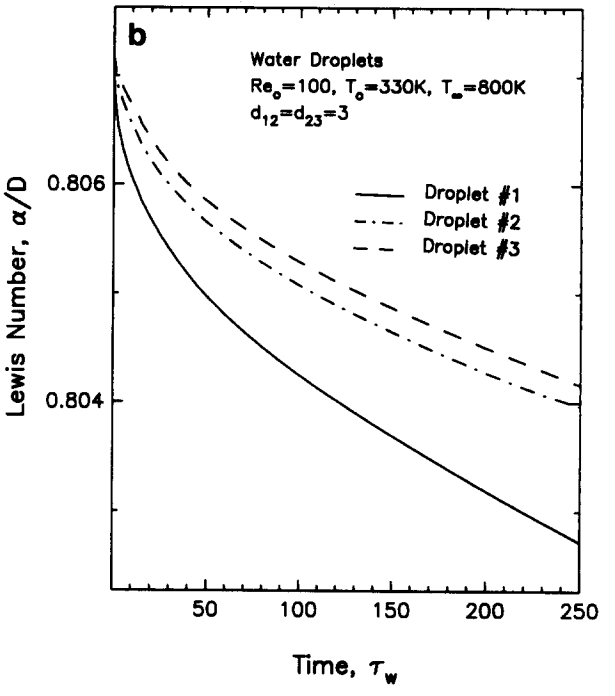

Figure 2(b) Transient Lewis numbers for water droplets (p_∞ = 1 atm)

Fuel droplet study

Figures 3 and 4 depict the time-dependent ($0.015\ \text{msec} \leq t_f^* \leq 0.220$ msec) gas-phase velocity vector plots and isotherms of three interacting vaporizing fuel droplets ($d_{of}^* = 50\ \mu m$). The second and third droplets approach in tandem the leading droplet, which experiences maximum drag and size reduction. The strong individual droplet wakes ($\tau_f = 10$) turn into weak recirculation regions ($\tau_f = 140$) because of droplet pairing and decreasing droplet Reynolds numbers (cf. Figures 3a–3c). For the given set of initial conditions, it is evident that during the

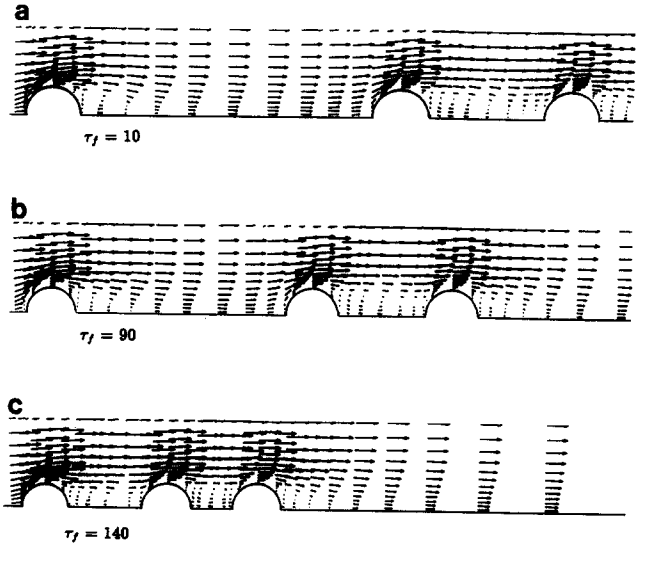

Figure 3 Gas-phase velocity vector plots, relative droplet positions and droplet shrinkage for n-hexane fuel at (a) $\tau_f = 10$, (b) $\tau_f = 90$, and (c) $\tau_f = 140$ ($Re_o = 100$, $p_\infty = 10$ atm, $T_\infty = 1200$ K, $T_o = 350$ K, $d_{12} = 6$, $d_{23} = 3$)

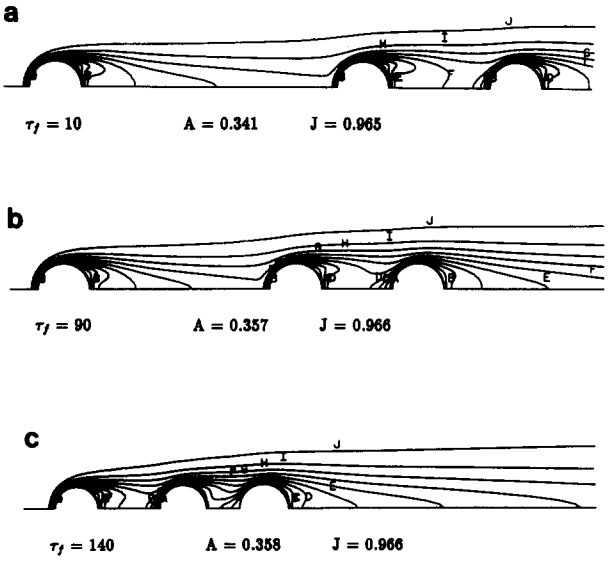

Figure 4 Gas-phase isotherms for three n-hexane fuel droplets at (a) $\tau_f = 10$, (b) $\tau_f = 90$, and (c) $\tau_f = 140$

later stages ($\tau > 140$) the third droplet affects the dynamics of the leading droplet via the center droplet. Thus, the present three-drop analysis is more realistic than previous one- or two-drop studies (cf. Renksizbulut and Haywood 1988; Chiang et al. 1989; Raju and Sirignano 1990). At $\tau_f > 160$, droplet collision can be expected. The different diffusion scales during the start-up phase, $\tau_f \leq 100$ (cf. Figure 2a), cause different boundary-layer thicknesses for heat and mass transfer. The relatively thick thermal boundary layers are indicated with the temperature contour plots in Figures 4a–4c. While thermal diffusion is still important in the (interfacial) heat transfer process, mass transfer is almost entirely dominated by convection effects. When droplet pairing occurs (cf. Figures 4b and 4c, e.g., at $\tau_f \approx 90$ for droplets 2 and 3 and at $\tau_f \approx 140$ for all three droplets), heat transfer is significantly reduced at the local interfaces because of the weakly recirculating, almost isothermal fluid.

The evolution of liquid-phase flow and heat transfer patterns, in terms of streamlines and isotherms of the leading droplet, are shown in Figures 5a–5d. Although the droplet formation process may generate a priori some internal circulation, zero vorticity is assumed at $\tau = 0$. After an initial start-up period ($\tau_f \approx 40$), the internal droplet circulation almost reflects Hill's vortex, at least for this particular set of conditions. The corresponding isotherms, however, exhibit a strong and longer dependence on the interaction between the gas-phase heat transfer and liquid convection. The constant-temperature contours are at first almost concentric due to *conduction*-dominated heat transfer; then, the heated liquid moves from the rear portion of the droplet toward the front stagnation point. During this time period, $10 < \tau_f < 30$, (unheated) liquid is convected from the interior to the droplet surface. In turn, this uniquely affects the interfacial quantities such as surface temperature, "blowing" velocity and fuel vapor concentration, and hence integral quantities such as the total drag, Nusselt number, and Sherwood number discussed elsewhere (Chiang and Kleinstreuer 1992). At about $\tau_f \geq 50$, the isotherms are largely determined by the strong internal circulation patterns.

Water droplet study

Next to fuels, water and polymers are the most common liquids used in droplet spray applications. In contrast to most fuels, which are rather volatile and possess high molecular weights, water sprays, having a higher heat capacity and dynamic viscosity, do not exhibit the dramatic changes in terms of two-phase flow patterns, heat transfer, vapor transfer, and droplet dynamics as, say, n- hexane sprays do. This is demonstrated in Figure 2b and again in Figures 6a–6c and Figures 7a–7c, although the initial conditions differ, naturally. Larger run times, i.e., $t_w^* = \tau_w$(1.178E-4)sec *versus* $t_f^* = \tau_f$(1.524E-6)sec, are required in order to show some interaction effects, for example, the approach of the second droplet toward the lead droplet ($d_{0,w}^* = 1$ mm). The third droplet stays at the initial spacing apart (cf. Figures 6a–6c). For the representative operational conditions chosen, droplet vaporization has no visible effect on the gas flow field and isotherms (cf. Figures 7a–7c).

The liquid-phase flow field, which establishes itself rather quickly, is moving very slowly while the conduction-dominated temperature field remains almost isothermal for $\tau_w \leq 200$, considering that the relative difference in the dimensionless temperature contour values remains at 0.001 (cf. Figures 8a and 8b).

Conclusions

The basic gas–liquid velocity and temperature fields of interacting vaporizing n-hexane fuel and water droplets have been analyzed for an initial Reynolds number of $Re_0 = 100$. Laminar axisymmetric flow and spherical droplets are the key assumptions for the present finite-element solution of the complete transport equations. The results of the two computer simulation studies for three n-hexane fuel droplets and three water droplets can be summarized as follows:

- Different diffusion rates are found for the heat and mass transfer of the evaporation of high-molecular-weight droplets such as n-hexane fuel. The stronger thermal diffusion mechanism is reflected in the thicker *thermal* boundary layer. The Lewis number is larger than unity during the initial phase, and hence the effects of variable fluid properties, especially on the liquid-phase viscosity, have to be accounted for. In contrast, the Lewis number of water droplets remains about constant, and fluid properties can be evaluated a priori at appropriate reference temperatures and vapor mass fractions.
- The relative motion between all three fuel droplets, and hence the resulting interaction effects, is largely dependent on the interfacial phenomena such as surface "blowing" (i.e., vaporization rates) and surface "slip" (i.e., tangential) velocity. The resulting two-phase velocity and temperature fields exhibit these transient effects of strong wakes when the droplets are far apart ($d_{ij} \geq 6$), weak recirculation regions or cavity formations when $d_{ij} \leq 2$, thicker momentum and thermal boundary layers due to droplet evaporation, and shear-stress-induced internal circulation, which tends to delay flow separation and creates a vortex-dominated liquid-phase temperature field.

  In contrast, for *water* droplets the shear-induced internal fluid motion, droplet heating, and hence the interfacial velocities are several orders of magnitude lower than for fuels, mainly because of water's contrasting properties. As a result, changes in differential transport phenomena and integral parameters and hence the dynamics of interacting vaporizing water droplets is much less dramatic and may take much longer to develop towards a steady state.
- The lead droplet and the second droplet exhibit the strongest interaction effects if the spacing between the second and third droplet is selectively large, e.g., $d_{23}|_0 > 3$ for n-hexane droplets at $Re_0 = \mathcal{O}(100)$. The fluid mechanics, heat transfer, and

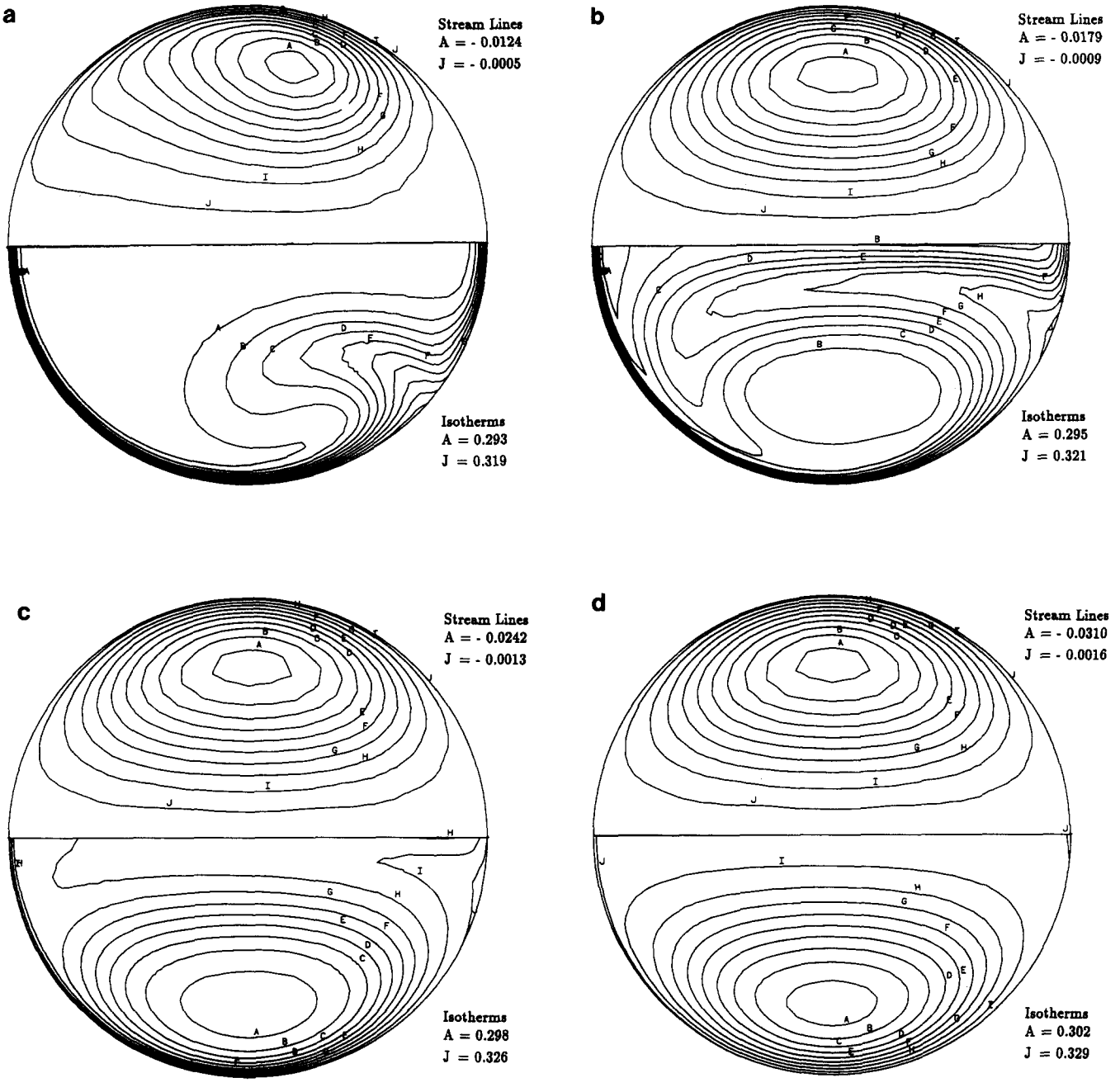

Figure 5 Liquid-phase stream lines and isotherms of leading n-hexane fuel droplet at (a) $\tau_f = 10$, (b) $\tau_f = 20$, (c) $\tau_f = 140$, and (d) $\tau_f = 90$ (cf. Figures 3 and 4)

mass transfer of each of the three *water* droplets on a 1-D trajectory are quite similar, especially in cases of sufficiently wide droplet spacings, i.e., $d_{13}|_o = d_{23}|_o > 2$.

Future work

Future work will concentrate on fundamental research as well as applied research aspects. Of basic interest are the effects of deforming droplets, gas-phase turbulence, and random droplet patterns on the multidroplet dynamics. Applied research work will focus on the development of practical spray parameter correlations describing the time histories of relative droplet velocity, and spacing for different initial Reynolds numbers, injection frequencies, liquids, and operational conditions.

Acknowledgments

This work has been supported in part by the Department of Energy, Office of Basic Energy Science, Grant No. DE-FG05-87ER13728. The assistance by the North Carolina Supercomputing Center (NCSC) under an Advanced Computing Resources Grant from the State of North Carolina is greatly appreciated. One of the authors (JKC) would like to acknowledge the support of a DOE-sponsored Computational Science Graduate Fellowship.

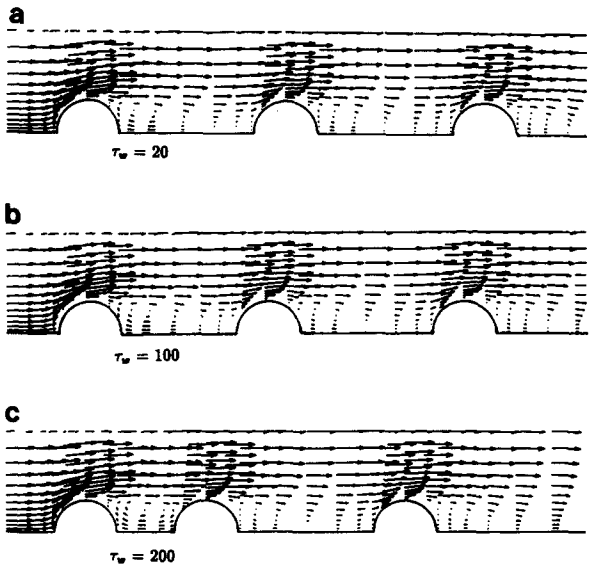

Figure 6 Gas-phase velocity vector plots, relative droplet positions, and droplet shrinkage for water at (a) $\tau_w = 20$, (b) $\tau_w = 100$, and (c) $\tau_w = 200$ ($Re_o = 100$, $p_\infty = 1$ atm, $T_\infty = 800$ K, $T_o = 330$ K, $d_{12} = 3$, $d_{23} = 3$)

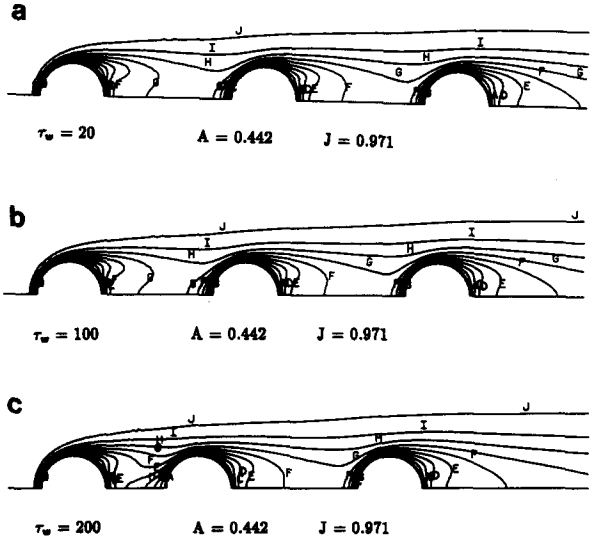

Figure 7 Gas-phase isotherms for three water droplets at (a) $\tau_w = 20$, (b) $\tau_w = 100$, and (c) $\tau_w = 200$

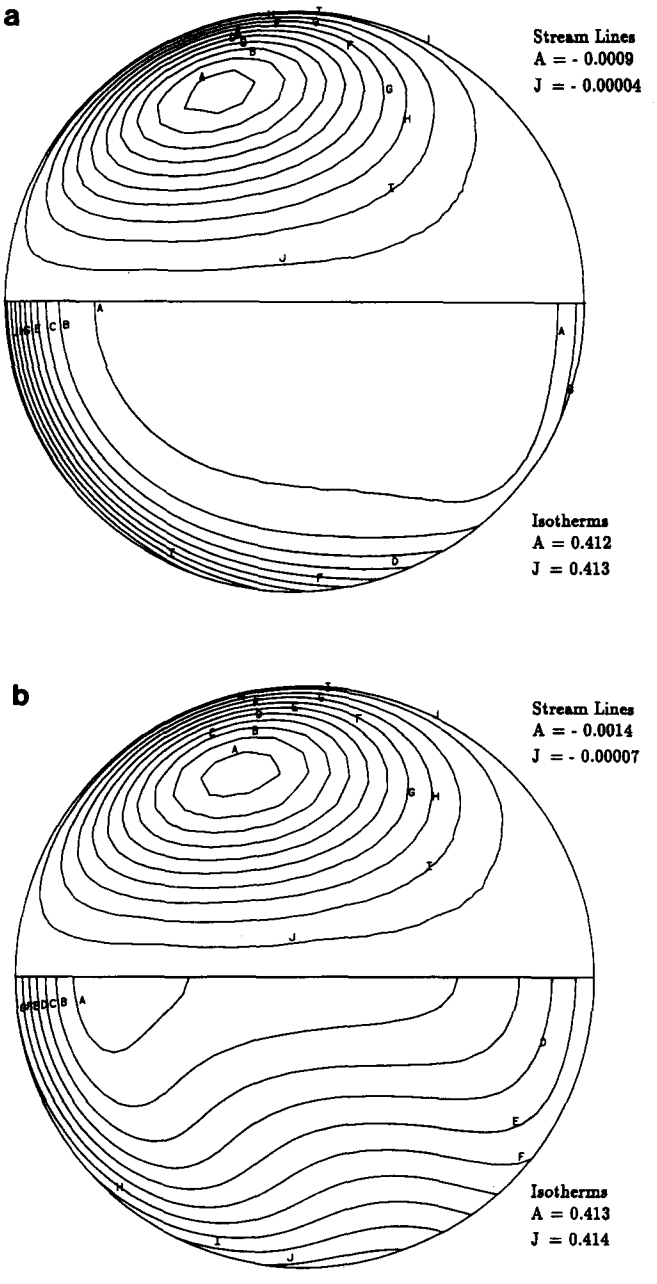

Figure 8 Liquid-phase stream lines and isotherms of leading water droplet at (a) $\tau_w = 20$ and (b) $\tau_w = 200$ (cf. Figures 6 and 7)

References

Abramizon, B. and Sirignano, W. A. 1988. Droplet vaporization model for spray combustion calculations. AIAA 26th Aerospace Science Meeting, Reno, NV

Bellan, J. and Harstad, K. 1987. Analysis of the convective evaporation of nondilute clusters of sprays. *Int. J. Heat Mass Transfer*, **30**, 125–136

Bracco, F. V. 1985. Modeling of engine sprays. SAE Technical Paper Series No. 850394, Washington, DC

Faeth, G. M. 1987. Mixing, transport and combustion in sprays. *Prog. Energy Comb. Sci.*, **13**, 293–345

Chiang, H. 1991. Numerical analyses of interacting spheres and vaporizing droplets. Ph.D. Thesis, Mechanical and Aerospace Engineering Department, North Carolina State University, Raleigh, NC

Chiang, H. and Kleinstreuer, C. 1992. Computational analysis of interacting vaporizing fuel droplet on a one-dimensional trajectory, *Combust. Sci. Technol.*, **86**, 289–309

Chiang, H. and Kleinstreuer, C. 1991. Convection heat transfer of colinear interacting droplets with surface mass transfer. *Int. J. Heat Fluid Flow*, **12**(3), 233–239

Chiang, C. H., Raju, M. S., and Sirignano, W. A. 1989. Numerical analysis of convecting, vaporizing fuel droplet with variable properties. 27th Aerospace Sciences Meeting (Paper #AIAA-89-0834), Reno, NV

Clift, R., Grace, J. R., and Weber, M. E. 1978. *Bubbles, Drops and Particles*. Academic Press, New York

Cuvelier, C., Segal, A., and Van Steenhoven, A. A. 1986. *Finite Element Methods and Navier–Stokes Equations*. D. Reidel, Dordrecht, Holland

Engelman, M. S. 1990. *FIDAP 5.0 Manuals Volumes 1 to 3.* FDI, Evanston, IL

Kleinstreuer, C. and Wang, T.-Y. 1990. Approximate analysis of interacting vaporizing fuel droplets. *Int. J. Multiphase Flow*, **16**(2), 295–304

Kleinstreuer, C., Wang, T.-Y., Chiang, H. 1990. Forced convection heat transfer of interacting solid spheres and vaporizing droplets. *In* T. N. Veziroglu (ed.), *Multiphase Transport & Particulate Phenomena*, Vol. 1. Hemisphere, New York, 461–492

Kleinstreuer, C., Wang, T.-Y., and Chiang, H. 1989. Interfacial heat and mass transfer of single and multiple drops in a hot gas stream. *In* R. K. Shah (ed.), *26th NHTC, ASME, Philadelphia, HTD*, Vol. 109. ASME, New York

Kuo, C. K. 1986. *Principles of Combustion.* Wiley-Interscience, New York

Law, C. K. 1990. Consideration of droplet processes in liquid hazardous waste incineration. *Combust. Sci. Technol.*, **74**, 1–15

Mulholland, J. A., Srivastava, R. K., and Wendt, J. O. L. 1988. Influence of droplet spacing on drag coefficient in nonevaporating, monodisperse streams. *AIAA J.*, **26**(10), 1231–1237

Raju, M. S. and Sirignano, W. A. 1990. Interaction between two vaporizing droplets in an intermediate Reynolds number flow. *Phys. Fluids A*, **2**(10), 1780–1796

Ramachandran, R. S., Kleinstreuer, C., and Altwicker, E. R. 1987. Mass transfer to an accelerating multidrop system. *Int. J. Heat Mass Transfer*, **30**(3), 607

Ramachandran, R. S., Wang, T.-Y., Kleinstreuer, C., and Chiang, H. 1991. Laminar flow past three closely-spaced monodisperse spheres or nonevaporating drops. *AIAA J.*, **29**(1), 43–51

Renksizbulut, M. and Haywood, R. J. 1988. Transient droplet evaporation with variable properties and internal circulation at intermediate Reynolds numbers. *Int. J. Multiphase Flow*, **14**(2), 189–202

Renksizbulut, M. and Yuen, M. C. 1983. Experimental study of droplet evaporation in a high-temperature air stream. *ASME J. Heat Transfer*, **105**, 384–388

Rowe, D. N. and Henwood, G. A. 1961. Drag forces in a hydraulic model of a fluidized bed. *Trans. Inst. Chem. Eng.*, **39**, 43–54

Sirignano, W. A. 1983. Fuel droplet vaporization and combustion theory. *Prog. Energy Comb. Sci.*, **9**, 291–322

Tal, R., Lee, D. N., and Sirignano, W. A. 1984. Heat and momentum transfer around a pair of spheres in viscous flow. *Int. J. Heat Mass Transfer*, **27**(11), 1953–1962

Tong, A. Y. and Chen, S. J. 1988. Heat transfer correlations for vaporizing liquid droplet arrays in a high-temperature gas at intermediate Reynolds number. *Int. J. Heat Fluid Flow*, **9**(2), 118–130

Tsuji, Y., Morikawa, Y., and Terashima, K. 1982. Fluid-dynamic interaction between two spheres. *Int. J. Multiphase Flow*, **8**, 71–82